Front. Optoelectron. China 2010, 3(2): 169–178
DOI 10.1007/s12200-010-0012-1

RESEARCH ARTICLE

Underwater image restoration by means of blind deconvolution approach

Fan FAN, Kecheng YANG (✉), Min XIA, Wei LI, Bo FU, Wei ZHANG

Wuhan National Laboratory for Optoelectronics, College of Optoelectronic Science and Engineering, Huazhong University of Science and Technology, Wuhan 430074, China

Abstract Although the use of blind deconvolution of image restoration is a widely known concept, little literatures have discussed in detail its application in the problem of restoration of underwater range-gated laser images. With the knowledge of the point spread function (PSF) and modulation transfer function (MTF) of water, underwater images can be better restored or enhanced. We first review image degradation process and Wells' small angle approximation theory, and then provide an image enhancement method for our underwater laser imaging system by blind deconvolution method based on small angle approximation. We also introduce a modified normalized mean square error (NMSE) method to validate the convergence of the blind deconvolution algorithm which is applied in our approach. The results of different initial guess of blind deconvolution are compared and discussed. Moreover, restoration results are obtained and discussed by intentionally changing the MTF parameters and using non-model-based PSF as the initial guess.

Keywords underwater imaging, image restoration, blind deconvolution, modulation transfer function (MTF), point spread function (PSF)

1 Introduction

Underwater image degradation is caused both by light propagation in water and the optical imaging system design, including lenses and recording devices. Rapid decay of signals due to absorption leads to poor signal-to-noise ratio (SNR), strong backscatter by the water itself together with underwater particles which dominantly induces the blurring of the image. Moreover, the inherent characteristic of imaging system brings about the additional noise on the underwater image. Image enhancement and restoration in order to extend the imaging range is important for many civilian and military applications, including target detection, search and rescue, and diver visibility [1].

Traditional method of image enhancement and restoration focuses on the image's own features. However, in underwater environment, without knowledge of any in-water transferring process involved or the optical properties, the effectiveness is considerably restrained [2]. Recent studies of Hou's group showed that the knowledge of in-water optical properties and their relationship to the image formation can be exploited in order to restore the imagery to the best possible level based on Wells' small angle approximation (SAA) [3]. The method proposed by them used imagery-derived modulation transfer function (MTF) as an estimation of image degradation, which was employed in an automated restoration framework for underwater imagery enhancement. Moreover, several types of point spread function (PSF) models were compared and validated by the same group, and a simplified semi-analytical form of PSF was proposed and implemented in underwater imaging restoration applications [4].

In this paper, our research deals with the image enhancement method for range gated underwater pulsed laser imaging system with intensified charge-coupled device (ICCD) camera. Utilizing this system, the back-scattered light of laser pulse is effectively reduced by the range gated technique, and therefore, the primary factor of image degradation is the blur of scattered photons travelling from the target to the receiver together with additive noise which is mainly caused by the gain of ICCD [5]. In our approach, noise reduction of underwater image is first proceeded, and then the deblurring procedure is taken by using analytical MTF of the water based on Wells' SAA. The theory of our approach is discussed in

Received December 22, 2009; accepted January 20, 2010

E-mail: kcyang@mail.hust.edu.cn

Sect. 2, the underwater imaging experiment results are outlined in Sect. 3, and comparison and discussion of restoration results are elicited in Sect. 4.

2 Blind deconvolution method based on SAA theory

2.1 Imaging model

Theoretically, assuming the imaging system is linear and spatially shift-invariant, then the degraded image of an object $g(x,y)$ can be described as

$$g(x,y) = h(x,y) \otimes o(x,y) + n(x,y), \tag{1}$$

where $\otimes$ denotes the two-dimensional (2-D) convolution of original image $o(x,y)$ and PSF $h(x,y)$ of degradation process, which represents the system response to a point source, and $n(x,y)$ is the additive noise. The system response includes those from both the imaging system itself as well as the effect of the medium. Applying Fourier transform on Eq. (1), the imaging model in the frequency domain is represented as

$$G(u,v) = H(u,v)O(u,v) + N(u,v), \tag{2}$$

where u and v are the spatial frequencies, and G, H, O, and N are the Fourier transform of g, h, o, and n, respectively. The system response function H in the frequency domain can also be comprehended as optical transfer function (OTF), the magnitude of which is MTF. Noticing that the term $H(u,v)$ is the total system response in the frequency domain and its cascading nature, it can be transformed into the multiplication of frequency response of multiple individual components in imaging application. Therefore, a multiplication expression of system response H is described as

$$H(u,v) = H_{\text{system}}(u,v)H_{\text{medium}}(u,v). \tag{3}$$

Applying inverse Fourier transform on Eq. (3), the total PSF of the imaging application can be described as

$$h(x,y) = h_{\text{system}}(x,y) \otimes h_{\text{medium}}(x,y). \tag{4}$$

2.2 Wells' SAA theory

When the angle of field of view (FOV) is less than 10°, the SAA theory is eligible in the acquisition of the transferring MTF in underwater environment. It is based on a linear time-dependent radiative transferring equation obtained by approximating $\sin\theta$ by θ and $\cos\theta$ by 1, where θ is the displacement from the unperturbed beam axis. With this approximation, the temporal dependence may be separated out, yielding a linear integro-differential equation describing the lateral spreading of the beam as it propagates through the media. In Wells' theory, assuming a cylindrical symmetry system, the PSF $h_{\text{medium}}(\theta,R)$ is related to the $H_{\text{medium}}(\psi,R)$ through the Hankel transform:

$$h_{\text{medium}}(\theta,R) = 2\pi \int J_0(2\pi\theta\psi) H_{\text{medium}}(\psi,R)\psi \mathrm{d}\psi, \tag{5}$$

$$H_{\text{medium}}(\psi,R) = 2\pi \int J_0(2\pi\theta\psi) h_{\text{medium}}(\theta,R)\theta \mathrm{d}\theta, \tag{6}$$

where ψ is the spatial frequency in cycles per radian, and R is the imaging distance. Furthermore, the relationship between the MTF and the inherent optical properties (IOPs) of the medium, e.g., scattering and absorption, is the key to the SAA. In general, the outcome of the optical imaging is determined by the scattering properties of the transmission medium. IOP is usually measured by the total scattering coefficient (b), which is equal to the product of total attenuation coefficient (c) and albedo (ω), determining the probability of a photon being scattered away from its original travelling direction per unit length by the medium molecules, constituents within the medium and turbulence [4]. Following this relationship, Wells explicitly derived the following formula:

$$b = c\omega, \tag{7}$$

$$H_{\text{medium}}(\psi,R) = \exp\left\{ -cR + bR\left[\frac{1-\exp(-2\pi\theta_0\psi)}{2\pi\theta_0\psi}\right]\right\}, \tag{8}$$

where the parameter θ_0 is referred to the median scattering angle for single scattering, and cR means the optical length. The PSF of the water is then obtained by numerical integration of Eq. (5).

2.3 Blind deconvolution approach

Most image restoration techniques are based on some prior knowledge of the image degradation; the point luminance and spatial impulse response of the system degradation are assumed known [4]. From the above discussion, the prior knowledge of underwater image restoration is the MTF of the water (magnitude of $H_{\text{medium}}(u,v)$) and the MTF of the imaging system (magnitude of $H_{\text{system}}(u,v)$), which can be predetermined and calibrated but lack analytical expression. However, the presence of various noises is not simply available and complicates these through-the-sensor techniques. The total degradation may be difficult to determine or time-varying in an unpredictable manner. Nonetheless, the limiting factor in the underwater environment is the scattering caused by particles in the water when present, and the optical system only plays a very minor rule. In such cases, information about the degradation must be extracted from the observed image either explicitly or implicitly. Under this condition, we restore the underwater image by

the blind deconvolution algorithm, which can be used effectively if only a few information about the distortion (blurring and noise) is known [6]. The algorithm maximizes the likelihood that the resulting image, when convolved with the resulting PSF, is an instance of the blurred image, and restores the image and the PSF simultaneously using an iterative Richardson-Lucy algorithm [7,8]. The blind deconvolution algorithm is described as [9]

$$h_{i+1}^{k}(x,y) = \left\{ \left[\frac{c(x,y)}{h_i^k(x,y) \otimes o^{k-1}(x,y)} \right] \otimes o^{k-1}(-x,-y) \right\} h_i^k(x,y), \quad (9)$$

$$o_{i+1}^{k}(x,y) = \left\{ \left[\frac{c(x,y)}{o_i^k(x,y) \otimes h^{k}(x,y)} \right] \otimes h^{k}(-x,-y) \right\} o_i^k(x,y). \quad (10)$$

In Eqs. (9) and (10), two Richardson-Lucy iterations are performed within one blind deconvolution iteration: one for object evaluation and the other for the PSF. At the kth blind iteration, it is assumed that the object is known from the $k-1$ iteration. The PSF $h^k(x,y)$ is then calculated for a specified number of Richardson-Lucy iterations, as in Eq. (9) above, where index i represents the Richardson-Lucy iteration. The kth guess of object $o^k(x,y)$ is calculated for the same number of Richardson-Lucy iterations. This is done by using the PSF evaluated from the full iteration of Eq. (9). The degraded image is again given as $c(x,y)$ in both Eqs. (9) and (10). The loop is repeated as required. With initial guesses $o_0^0(x,y)$ made for the object and the PSF $h_0^0(x,y)$, the estimate of the original image and total PSF can be obtained after a given time of iterations. The whole iterative process can use fast Fourier transform to reduce the computation burden.

Traditionally (i.e., in astronomy applications), the above algorithms are not sensitive to the shape of PSF, but in underwater image restoration, the influence of shape variation of initial PSF on deconvolution results must be validated. In Eq. (8), when the albedo ω and θ_0 are selected, $H_{\text{medium}}(\psi,R)$ is the function of optical length cR and spatial frequency ψ, so the shape of PSF is only affected by the optical length and supported size selected in Cartesian coordinates. Furthermore, in many image restoration applications, the degraded image is commonly generated by convolving an original image with a known PSF, and then the blind deconvolution is performed to determine the best iteration number compared with the original image (regarded as a reference image) based on measuring normalized mean square error (NMSE). However, the ideal image could not be obtained in underwater environment, so we introduce a modified NMSE expression to evaluate the convergence of the blind deconvolution algorithm and discuss the influence of iteration number selection on the restoration result. The modified NMSE expression is described as

$$\xi_t = \frac{\sum_{j=1}^{J}\sum_{l=1}^{L} |o_t(j,l) - o_{t-1}(j,l)|^2}{\sum_{j=1}^{J}\sum_{l=1}^{L} |o_1(j,l) - o_0(j,l)|^2}, \quad (11)$$

where suffix t means the total iteration time, which is equal to the multiplication of selected inner iteration number and outer iteration number in Eq. (10), and J and L represent the pixel numbers in two dimensions of the image, respectively. Here, o_0 is an equivalence expression of initial guess $o_0^0(x,y)$ made for an object. In this case, the mean square error is a function of total iteration time and normalized by its first iteration result.

Another factor which will affect the restoration result is the initial guess made for the object. In our approach, the denoised image is used as the initial guess for an object compared with choosing an original underwater image as the input. The noise pattern is analyzed, and noise reduction is performed by choosing the arithmetic mean filter with size 3×3, which is well suited for random noise like Gaussian or uniform noise and preserves the image details to a great extent simultaneously [10].

3 Underwater imaging experimental result

The underwater images were obtained at the basin of our college during March 2008 using the Range Gated Underwater Laser Imaging System which incorporated 532-nm pulsed lasers as the light emission source and ICCD of PI-MAX/MAX2 serials as the imaging device. A Q-switch signal from the laser controller was used to externally trigger the programmable timing generator (PTG) of the ICCD controller (ST-133) and controlled the gate shutter status; the data information was collected by the ST-133 and transferred to a computer for analyzing, and the underwater image could be viewed simultaneously through the software of the system.

The photograph of the target is shown in Fig. 1(a). It is a stripe resolution board with black ground color, which is 2 m long and 1 m wide covered by white banding frame and regularly distributed white stripes with various breadth starting from 15 cm (top) to 1 cm (right bottom). The target is located underwater at a distance of 30 m from the imaging system; the angle of FOV is approximately 4°, which is in the range limitation of Wells' theory ($0° < \theta < 10°$); a frequency-doubled, Q-switched Nd:YAG laser produced linear polarized green light in an 8-ns pulse at a rate of 1 Hz. The pulse energy was 100 mJ at 532 nm; the gain of the ICCD was 100, and the gate width was 10 ns. The attenuation coefficient measured was 0.27 m^{-1}, and the

albedo was 0.8 suggesting that the optical length was 8.1. The underwater image (original size 1340×1300, resized to 268×260) of the target obtained on March 10th, 2008 is shown in Fig. 1(b).

Remarkably, the image showed in Fig. 1(b) has four black areas which resulted from the optical imaging system: the field of view of the system did not fully cover the ICCD's imaging area, inducing a circular image appearance within a black square boundary. However, the gray scale of the four black areas is not zero, which is brought by the ICCD's current noise and will be of assistance to us to perform the noise reduction process.

4 Image restoration result and discussion

4.1 Restoration result of distinct initial guesses for an object

First, we perform image restoration by a blind deconvolution algorithm dealing with the original image directly. With the parameters obtained, the medium MTF is calculated and normalized following Eq. (8) by assuming the median scattering angle for single scattering $\theta_0 = 0.03°$; then the PSF with size of 101×101 array embedded in a 268×260 array of zeros is obtained by Eq. (5). The calculated medium MTF curve and restored MTF curve is shown in Fig. 2(a), while the total iteration number is 50. The restored underwater image of Fig. 1(b) is provided in Fig. 2(b), and the edge extraction result of the restored image is shown in Fig. 2(c). When the blind deconvolution approach is applied without a prior denoising disposal, the processed image exhibits improvements both in details and contrast, but the noise ingredients are intensified simultaneously. Moreover, the spacing between the calculated MTF curve and the restored MTF curve illustrates that, although the resolution is increased after restoration, the magnification of noise attenuates this effect, inducing coarse contour of the edge extraction result, which is a disadvantageous factor in underwater imaging enhancement, and the noise reduction must be preprocessed.

Therefore, we cut out the top-left part of the dark area from the original image and generate its gray-scale histogram, which is showed in Fig. 3(a). The Gaussian pattern of noise distribution is assumed according to the approach provided by Ref. [10].

Consequently, noise reduction is performed according to the approach discussed in Sect. 2.3. The denoised image is then obtained as the initial estimation of the blind deconvolution approach, which is shown in Fig. 3(b). Figure 4 shows the MTF curves and the restored image after 50 times of total iteration. When the noise reduction method is applied, the restored image shows significant improvements both on details and contrast, with noise restrained in a visually acceptable range. However, on the bottom-right area of the target, the white stripes of narrower size are still indiscernible, which suggests that the enhancing effect does not perform remarkably in the high spatial frequency region of the image. This can be explained from the MTF curve that in the high spatial frequency area, the normalized values of the calculated medium MTF and restored MTF are close to zero, and their differentiation varies slightly. Therefore, the method proposed here exhibits better restoration effect compared with direct blind deconvolution when synthetically considering the contrast, details and noise, which can be proved by the result of a smoother contour in the edge extraction image shown in Fig. 4(c).

4.2 Restoration result of a different total iteration number

By selecting the denoising image shown in Fig. 3(b) as the initial object guess and maintaining other parameters unchanged, the restored image after 200 times iteration is

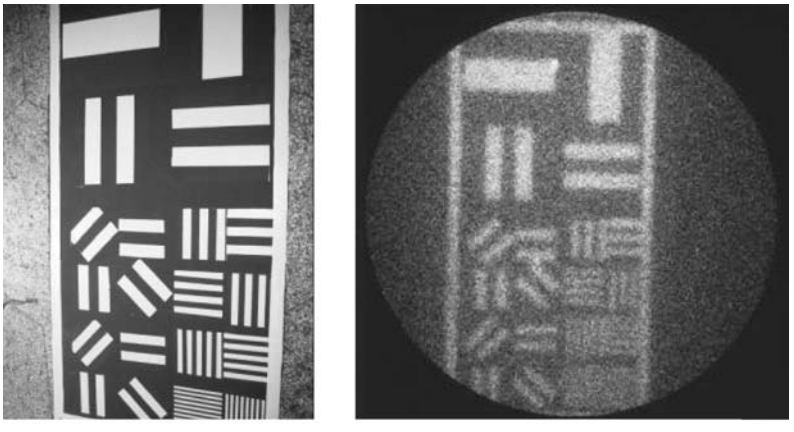

Fig. 1 (a) Target photograph; (b) underwater image of target

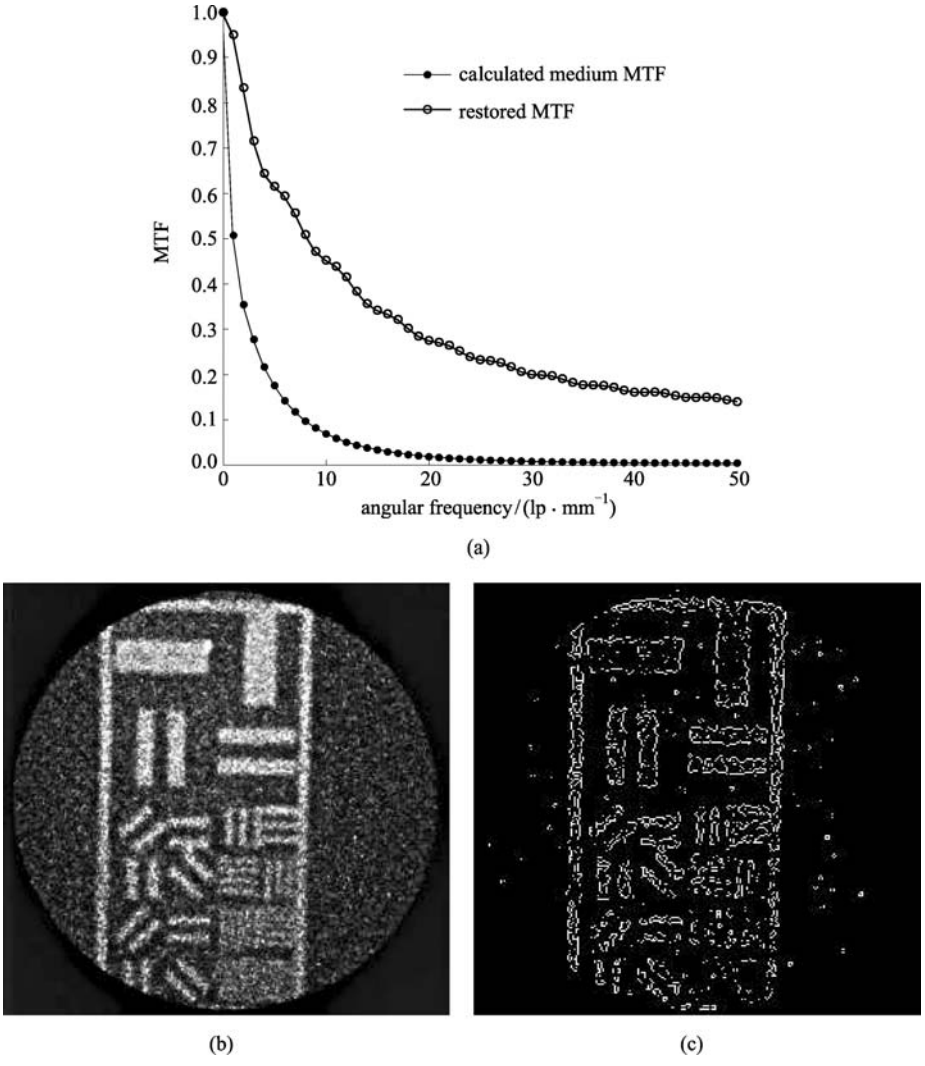

Fig. 2 (a) MTF curves (the total iteration number is 50); (b) restored image; (c) edge extraction result

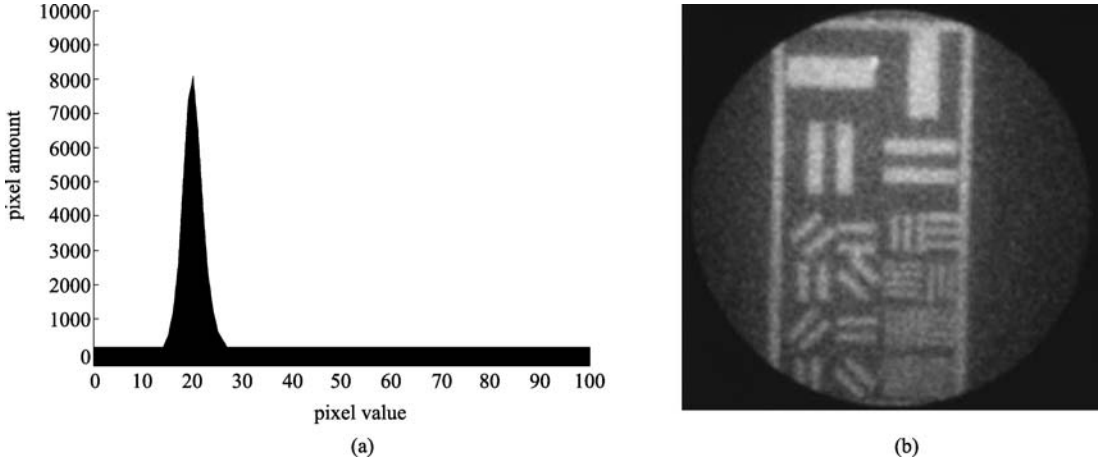

Fig. 3 (a) Histogram of selected dark area; (b) denoising image

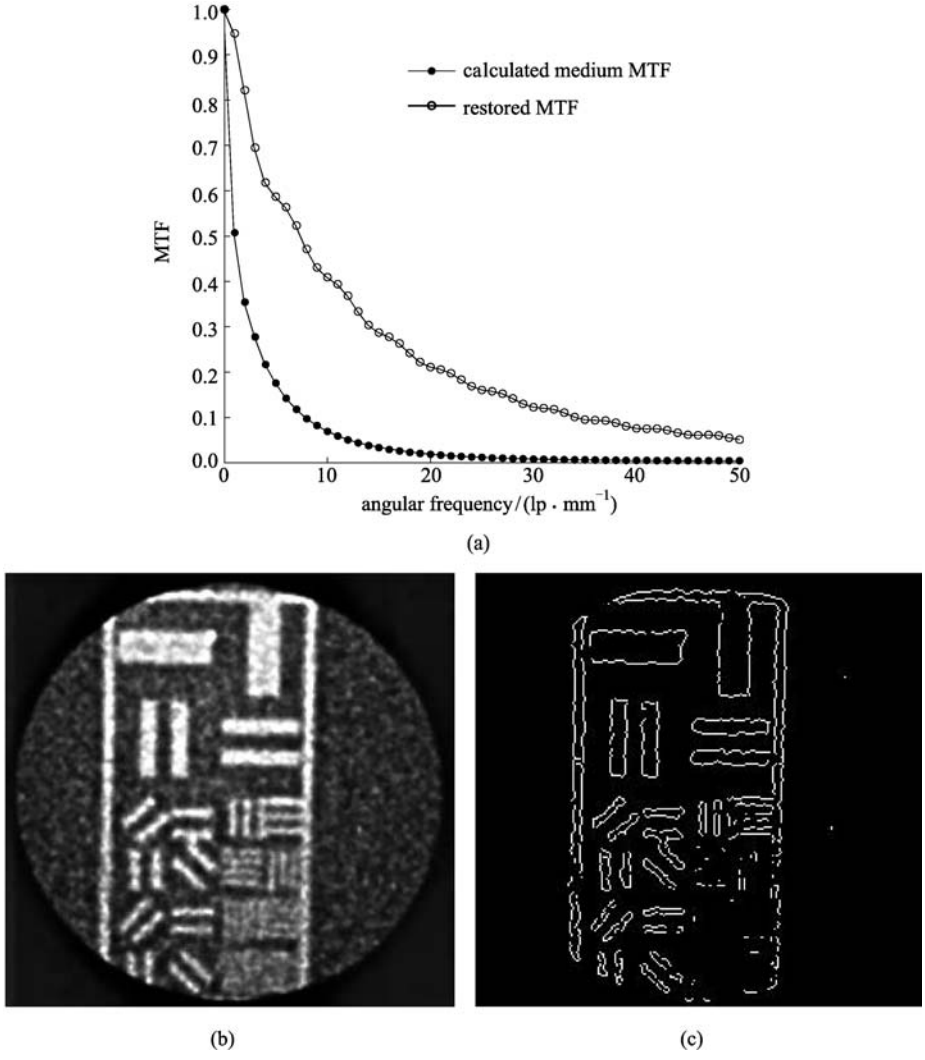

Fig. 4 (a) MTF curves when noise reduction method is applied; (b) restored image; (c) edge extraction result

shown in Fig. 5(a), and the modified NMSE curve is shown in Fig. 5(b) according to Eq. (11). It is found that after tens of times of iteration, the blind deconvolution algorithm tends to converge, which results from the NMSE being close to zero. However, the fact that the restored image does not reflect a better effect in contrast and details and noise is amplified suggests that this algorithm has worse noise tolerance under a large iteration number. Although the restored MTF curve of 200 times iteration ascends, which is shown in Fig. 5(c), illustrates the details improvement in the restored image, the amplification of noise neutralizes the effect and decreases the contrast. In addition, a common criticism of mean-square error and least-squares error measures is that they do not always correlate well with human subjective testing [11]. Therefore, when the PSF size is selected as 101×101 array, we choose the total iteration number to be 50 for a balance among details, contrast, noise and human vision.

4.3 Restoration result of different size of initial PSF guesses

In order to study the influence of different size of initial PSF guesses on restoration effect, we select two distinct sizes for the initial PSF guess: one is a 21×21 array, and the other is a 201×201 array. The calculated medium MTF and restored MTF curves are shown in Fig. 6(a) with the same half width for comparison convenience, and the restored images are shown in Figs. 6(b) and 6(c). Both iteration times are 50, and the input object guess is from Fig. 3(b). When the size of the input PSF is set smaller, more details of the image could be distinguished while noise is amplified on the image. This can be explained from the MTF curve: the high spatial frequency value of the restored MTF curve becomes larger, and therefore, the details of the image appear clearer, but the contrast is still low due to the dominance of the high-frequency noise. Furthermore, when a larger input PSF is set, the noise is

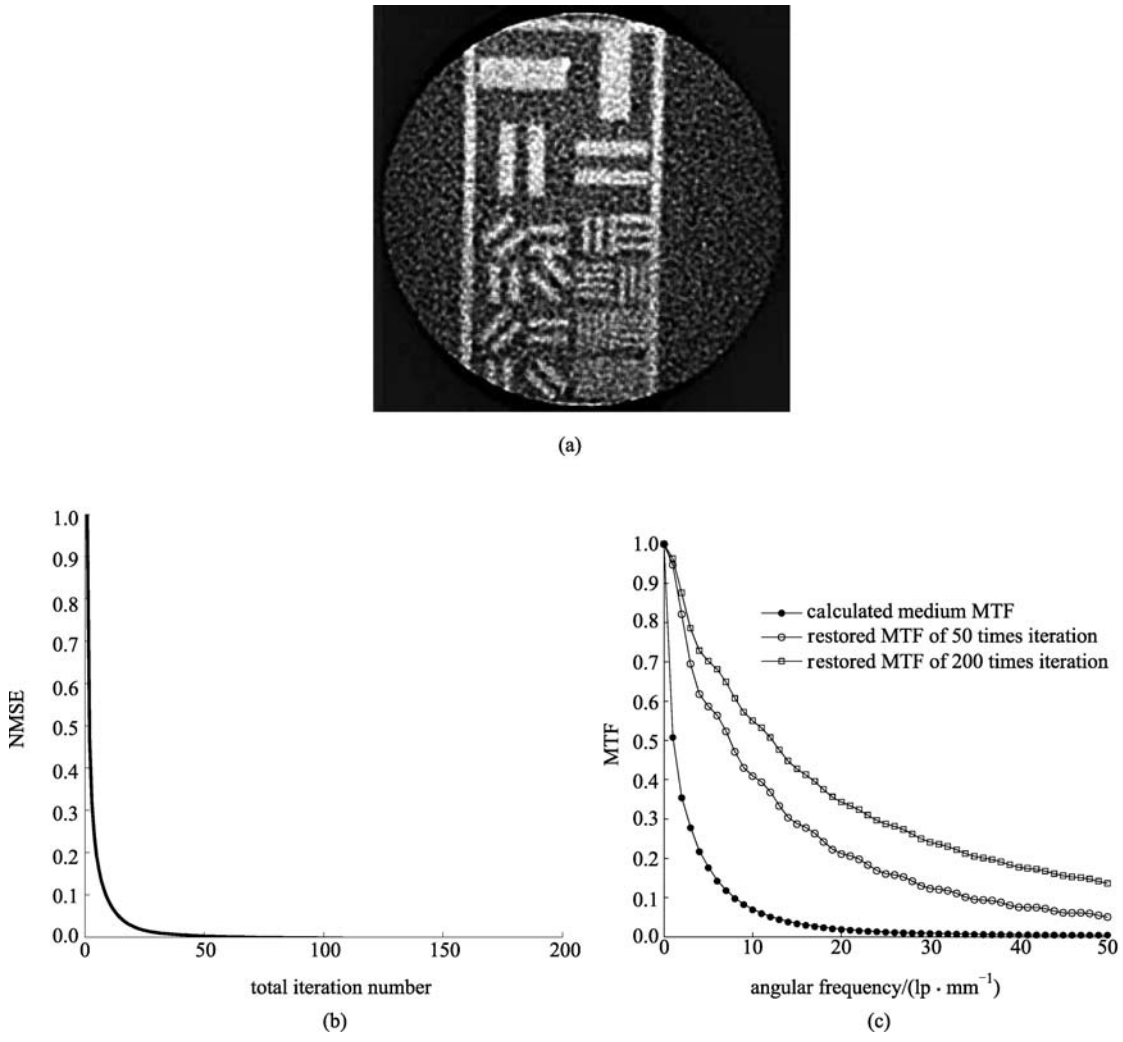

Fig. 5 (a) Restored image after 200 times of iteration; (b) NMSE curve; (c) MTF curves

restrained more effectively, whereas details improvement is not obvious, and the contrast enhancement effect is less than the result shown in Fig. 4(b). Therefore, the input PSF size determination is an important factor on the restoration result. Appropriate size selection will be assistance for obtaining a better restoration result based on the balance among details, contrast, noise and human vision. It is found that the image with a size of 268×260 pixels used in our approach performs well in blind deconvolution restoration when the initial PSF size is set to 101×101 array, and iteration time is selected as 50. This inference may be valuable for initial PSF size evaluation in other image restoration approach using the same blind deconvolution algorithm when the image size varies.

4.4 Restoration result under different optical length assumption

For the purpose of studying the impact of the shape variation of initial MTF on the image enhancement result, we calculate other two pairs of MTF curves using the same parameters in Sect. 4.2, but assuming a different optical length ($cR=2.7$ and $cR=21$ instead of 8.1). The calculation results of the MTF curves and corresponding images generated are shown in Fig. 7. When the optical length is assumed shorter than the actual one, the restored MTF curve locates away from the coordinate axis, and spacing between the modeled MTF and the restored MTF becomes in a far range. This variation can be apparently observed from the corresponding restored image results: the fact that a high spatial frequency value of the restored MTF becoming larger induces the clearer details of the restored image, but the dominance of the high-frequency noise masks this effect and causes a low contrast. On the contrary, when assuming longer distance, we notice actual degradation in details due to over-correction, especially at the circular border on the image, although contrast is still improved, and the high-frequency noise is restrained. This illustrates that when tested with intentionally different MTF (the PSF then alters), the result

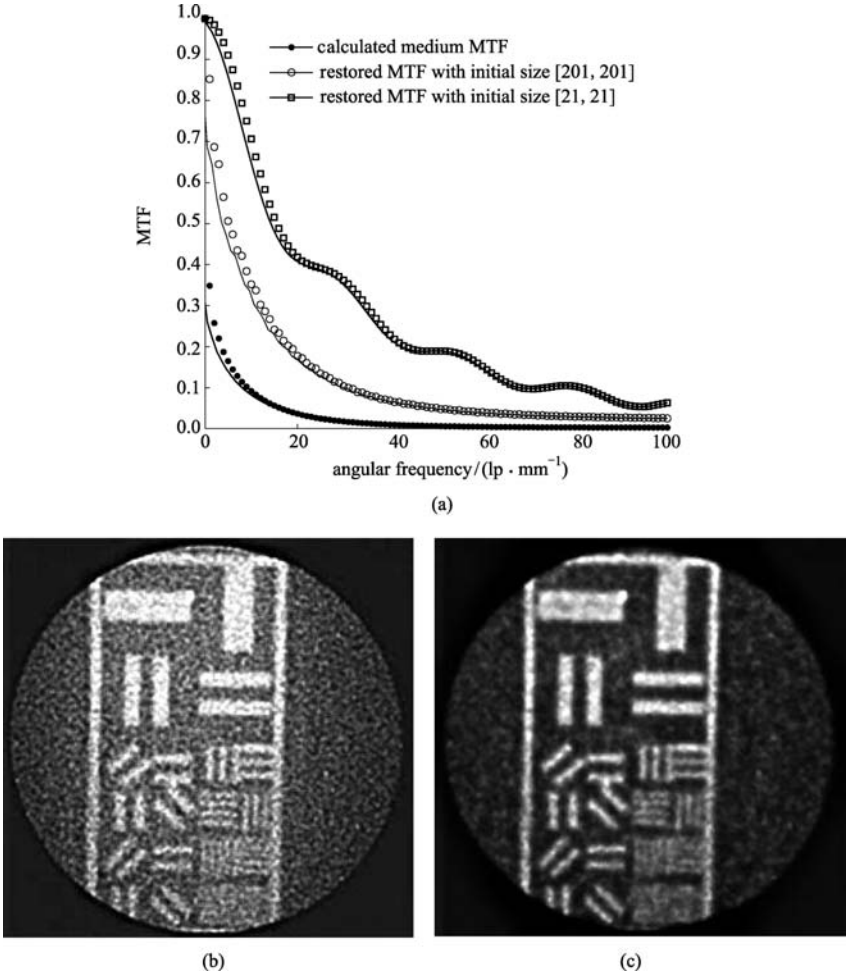

Fig. 6 (a) MTF curves of different size of initial PSF guesses; (b) restored image of input PSF with size 21×21 array; (c) restored image of input PSF with size 201×201 array

varies apparently, even though traditionally (i.e., in astronomy applications), such algorithms are not sensitive to the shape of PSF [9].

4.5 Comparative study of restoration result using non-model-based initial PSF guess

To further validate the importance of the PSF model, we choose some non-model-based PSF as the initial guess. Blind deconvolution is performed by using a denoising image shown in Fig. 3(b) as the object guess, starting with a 21×21 array of ones embedded in a 268×260 array of zeros for the initial PSF. The restored image is shown in Fig. 8(a), and the result is apparently worse, although this initial PSF option is always used in astronomical application [12]. We also choose Gaussian PSF as the initial guess, and the result is shown in Fig. 8(b). The ringing effect appears in the figure, especially the circular pattern near the boundary. However, this effect does not occur when using our modeled PSF, even if the parameters of the modeled PSF vary substantially. These examples further demonstrate the importance and validity of the correct PSF model to underwater image restorations. Moreover, even when the in-water parameters may not be measured precisely, the underwater image enhancement method provided in this paper still can be used by fine-tuning the parameters to obtain the proper MTF and the optimized restored image, which will assist the in-water parameters quantification in return.

5 Conclusion

An underwater image restoration method based on the Wells' small angle scattering theory and blind deconvolution approach is studied. The basic noise pattern of the image is analyzed, and the arithmetic mean filter is used first to perform image denoising; then, an iterative blind deconvolution method is performed using the denoised image as the initial guess of the ideal image and the PSF

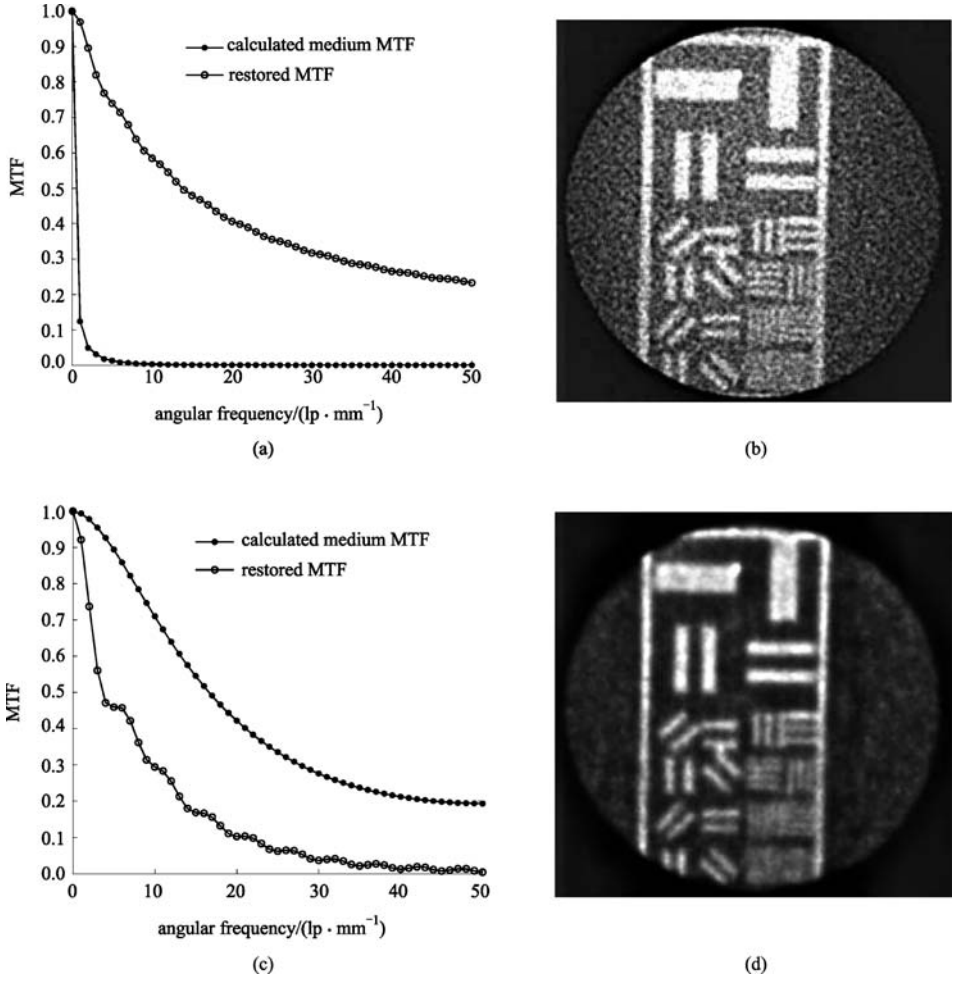

Fig. 7 (a) MTF curves (cR = 2.7); (b) restored image (cR = 2.7); (c) MTF curves (cR = 21); (d) restored image (cR = 21)

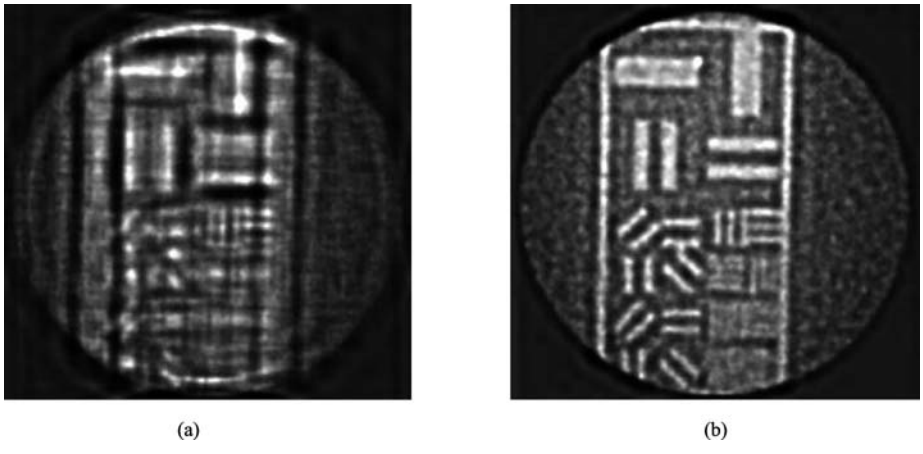

Fig. 8 (a) Restored image of initial PSF with 21×21 array of ones; (b) restored image of Gaussian initial PSF

calculated from the modeled MTF as the initial guess of the actual PSF. A modified NMSE model is introduced to evaluate the convergence of the blind deconvolution algorithm and assists to determine the iteration number

for better restoration result. The result shows that by the denoising preprocessing, the image enhancement effect is better than the result of directly employing the original image as the initial guess of the blind deconvolution. This demonstrates in part that the blind deconvolution algorithm can not perform noise restraint effectively in our underwater imaging applications, which leads to the further study of the noise generation and its reduction method of range gated underwater laser imaging system. Moreover, different restoration results are compared due to the different MTF data by intentionally changing the modeled MTF parameters or using non-model-based initial PSF. The result suggests that the blind deconvolution algorithm is sensitive to the variation of PSF in our application, which demonstrates the importance and validity of the correct MTF and PSF model to underwater image restorations. Finally, although the optical system only plays a very minor rule in optical imaging, further research will be conducted in the area of comparative study among other blind deconvolution algorithms, taking account of the total MTF of the optical imaging system, including modeled in-water MTF and the MTF of the optical imaging system.

References

1. Hou W, Lee Z, Weidemann A D. Why does the secchi disk disappear? An imaging perspective. Optics Express, 2007, 15(6): 2791–2802
2. Hou W, Gray D J, Weidemann A D, Fournier G R, Forand J L. Automated underwater image restoration and retrieval of related optical properties. In: Proceedings of IEEE International Geoscience and Remote Sensing Symposium. 2007, 1889–1892
3. Wells W H. Theory of small angle scattering. AGARD Lecture Series, 1973, 61
4. Hou W, Gray D J, Weidemann A D, Arnone R A. Comparison and validation of point spread models for imaging in natural waters. Optics Express, 2008, 16(13): 9958–9965
5. Moran S E, Ulich B L, Elkins W P, Strittmatter R J, DeWeert M J. Intensified CCD (ICCD) dynamic range and noise performance. Proceedings of SPIE, 1997, 3173: 430–457
6. Lane R G. Blind deconvolution of speckle images. Journal of the Optical Society of America A, 1992, 9(9): 1508–1514
7. Richardson W H. Bayesian-based iterative method of image restoration. Journal of the Optical Society of America, 1972, 62 (1): 55–59
8. Lucy L B. An iterative technique for the rectification of observed distributions. The Astronomical Journal, 1974, 79(6): 745–754
9. Fish D A, Brinicombe A M, Pike E R, Walker J G. Blind deconvolution by means of the Richardson-Lucy algorithm. Journal of the Optical Society of America A, 1995, 12(1): 58–65
10. Gonzalez R C, Woods R E. Digital Image Processing. New Jersey: Prentice Hall, 2002
11. Pratt W K. Digital Image Processing: PIKS Scientific Inside. 4th ed. New Jersey: Wiley-Interscience, 2007
12. Zhang J, Zhang Q, He G. Blind deconvolution: multiplicative iterative algorithm. Optics Letters, 2008, 33(1): 25–27